

## RESEARCH ARTICLE

10.1002/2013JE004496

## Key Points:

- Magma ocean crystallization would likely not cause degree-one overturn in Mars
- Postoverturn entrainment enables diverse reservoirs to participate in melting
- Thermal diffusion plays a key role in overturn timescales

## Correspondence to:

A. Scheinberg,  
scheinberg@mit.edu

## Citation:

Scheinberg, A., L. T. Elkins-Tanton, and S. J. Zhong (2014), Timescale and morphology of Martian mantle overturn immediately following magma ocean solidification, *J. Geophys. Res. Planets*, 119, doi:10.1002/2013JE004496.

Received 4 AUG 2013

Accepted 22 JAN 2014

Accepted article online 4 FEB 2014

## Timescale and morphology of Martian mantle overturn immediately following magma ocean solidification

A. Scheinberg<sup>1</sup>, L. T. Elkins-Tanton<sup>2,1</sup>, and S. J. Zhong<sup>3</sup>

<sup>1</sup>Department of Earth, Atmospheric, and Planetary Sciences, Massachusetts Institute of Technology, Cambridge, Massachusetts, USA, <sup>2</sup>Department of Terrestrial Magnetism, Carnegie Institution, Washington District of Columbia, USA, <sup>3</sup>Department of Physics, University of Colorado Boulder, Boulder, Colorado, USA

**Abstract** Energy of accretion in terrestrial planets is expected to create liquid silicate magma oceans. Their solidification processes create silicate differentiation and set the initial mantle structure for the planet. Solidification may result in a compositionally unstable density profile, leading to cumulate Rayleigh-Taylor overturn if a sluggish rather than stagnant lithosphere existed in the early stages of planetary history. The pattern and timescale of overturn, in which cold, dense surface material sinks to the core-mantle boundary, have implications for core dynamo production, volatile escape, and fundamental differences between differently sized bodies. Our fully spherical mantle models reaffirm previous work suggesting that harmonic degree of overturn is dependent on viscosity contrast and layer thickness. We find that cumulate overturn would likely have occurred with short wavelengths. In an isoviscous model, thermal convection ensues rapidly after overturn; however, when viscosity is temperature dependent, compositional stability in the mantle suppresses the onset of whole-mantle thermal convection. For a viscosity of  $10^{18}$  Pa s, the mantle could fully overturn in as little as 3 Ma.

### 1. Introduction

Estimates of gravitational potential energy converted into heat during Martian planetary accretion are as high as  $4 \cdot 10^{30}$  J [Wetherill, 1990], more than sufficient to melt the entire silicate mantle and produce a magma ocean. Given the short time period over which accretion may have occurred ( $10^5$  years) [Wetherill and Inaba, 2000] and further heating from radioactive decay and core differentiation, Mars's mantle may have become wholly or partially molten [e.g., Solomon, 1979]. The depth of this magma ocean is still not well constrained, with estimates based on geochemical evidence varying from 700 km [Richter et al., 1998] to greater than 1350 km [Debaille et al., 2008]. Isolated magma ponds due to large impacts are also a possibility [Tonks and Melosh, 1993]. In this study we consider the end-member case of a completely melted mantle.

A magma ocean is likely to become homogenous and adiabatic through convection. As the mantle's adiabatic temperature profile cools, the mantle will begin to crystallize. This will occur where the temperature profile intersects the solidus, initially at the base of the mantle and moving upward as the mantle continues to cool. These newly formed minerals are denser than the homogenous liquid and will thus precipitate out of the magma ocean [Martin and Nokes, 1989; Marsh, 1995] and form layered cumulates. The change in bulk composition in the liquid as cumulates solidify will result in a nonuniform density profile by the time the entire mantle has resolidified [Elkins-Tanton et al., 2003]. Magnesium-bearing minerals will crystallize preferentially, enriching the remaining melt in iron and, to a lesser extent, titanium and chromium. As the remaining progressively enriched melt solidifies, the resulting minerals will be progressively denser; this will result in a gravitationally unstable density profile.

At least until its later stages, the solidification of the magma ocean would likely occur before the solid material begins to equilibrate gravitationally, as the timescale of large-scale solid mantle advection is greater than that of fractional crystallization [Elkins-Tanton et al., 2005]. Since heat advection has not significantly progressed, temperatures immediately after solidification can be assumed to be the same as when the material solidified. The resulting temperature profile is the fractional solidification solidus. This temperature profile will enhance the gravitational instability and would possibly lead to overturn even in the absence of fractionation [Solomatov, 2000].

Provided a sufficiently low viscosity, the gravitationally unstable profile will result in spontaneous overturn of the mantle to reach a more gravitationally stable state. This process proceeds by Rayleigh-Taylor instability. Insights into the process can be made by considering the basic scenario in which a homogenous fluid is overlain with another homogenous fluid of higher density.

Computational and analytic studies in spherical geometry demonstrate that, for a given density structure, high viscosity contrast between layers results in a longer overturn wavelength [Parmentier *et al.*, 2002; Zhong and Zuber, 2001; Ke and Solomatov, 2006]. In a planetary interior, the longest wavelength, degree-one overturn, would correspond to a single large downwelling of dense material. Low viscosity contrasts result in higher degree overturn, with multiple smaller downwellings. However, a full three-dimensional model calculation has not yet been performed to confirm that those cases could be relevant to planetary mantles. Layer thickness also influences wavelength of overturn [Zhong and Zuber, 2001]. The thinner either layer becomes, the more difficult it is to acquire long-wavelength, degree-one instabilities.

Overturn and resulting mantle behavior could help explain puzzling characteristics of Mars. Degree-one overturn is of particular interest for Mars since the Martian crust demonstrates a degree-one dichotomy in (among other things) its remanent magnetization. While no dynamo is currently active in the Martian core, the northern hemisphere's crust is weakly magnetized, while the southern hemisphere's crust contains regions of both strong and weak magnetization [Zuber, 2001]. Degree-one overturn may potentially explain these features. A degree-one cold downwelling which arrives at the core-mantle boundary (CMB) could result in a high heat flux from the core in a single hemisphere. It has been shown that this heat flux distribution on the CMB could force the liquid outer core into a mode of convection leading to the production of a single-hemisphere dynamo [Stanley *et al.*, 2008]. If it was active in the southern hemisphere, such a dynamo could explain the observed remanent field. A giant impact has also been proposed as an alternative mechanism responsible for the dichotomy [e.g., Andrews-Hanna *et al.*, 2008].

Chemical observations may also be explained by the overturn process. Isotopic studies of the SNC meteorites, believed to be of Martian crustal origin [e.g., Treiman *et al.*, 2000], indicate that separate source reservoirs differentiated early on and remain separate [Jones, 1986; Borg *et al.*, 1997]. The nakhlite and chassigny meteorites point to a source region depleted in incompatible elements, while the source region inferred from several shergottites would have been enriched in them. Fractional crystallization of a magma ocean could explain the creation of these isotopic reservoirs. An overturn event could then separate and maintain them [Elkins-Tanton *et al.*, 2005]; however, details of their formation, structure, and behavior have yet to be understood.

Cumulate overturn will result in a more gravitationally stable mantle, which will initially stifle thermal mantle convection until the buoyancy force due to the thermal gradient is great enough to overcome compositional stability [Zarnek and Parmentier, 2004]. The early stages of mantle history, from solidification to the eventual initiation of convection, may have a profound influence on the future development of a planet. Mantle behavior will govern the production of an early atmosphere through volatile escape and define the properties of an early crust [Elkins-Tanton, 2008]. When and how thermal convection becomes dominant over chemical convection will vary greatly from planet to planet, as different fundamental characteristics (size, composition, etc.) determine how fractional crystallization will proceed and thus determine the relative strengths of chemical and thermal buoyancy.

This study simulates mantle dynamics in Mars from the completion of magma ocean solidification to a compositionally stable state and considers the lifetime of such a stably layered system. We will test previous two-dimensional work done on two-layer Rayleigh-Taylor overturn scenarios using a fully spherical geometry, and then explore possible overturn scenarios with more realistic planetary characteristics. In particular, we seek to (1) determine the spherical harmonic degree with which colder surface material advects downward during initial Rayleigh-Taylor overturn, (2) estimate the increase in core heat flux due to the overturn, (3) determine the resulting distribution of chemically distinct zones within the mantle, and (4) constrain the timescale of overturn and of subsequent convection-driven compositional homogenization for different possible viscosity profiles.

**Table 1.** Model Parameters

Parameter	Description	Value	Unit
$R$	Radius	$3396 \cdot 10^3$	m
$R_{\text{CMB}}$	Core radius	$1396 \cdot 10^3$	m
$\rho_o$	Reference density	3350	$\text{kg m}^{-3}$
$\Delta\rho_{\text{ch}}$	Chemical density variation	130	$\text{kg m}^{-3}$
$g$	Reference gravity	3.71	$\text{m s}^{-2}$
$c_p$	Specific heat	1250	$\text{J kg}^{-1} \text{K}^{-1}$
$\kappa$	Thermal diffusivity	$1 \cdot 10^{-6}$	$\text{m}^2 \text{s}^{-1}$
$\alpha$	Thermal expansivity	$3 \cdot 10^{-5}$	$\text{K}^{-1}$
$V$	Effective activation volume	$1.7 \cdot 10^{-6}$	$\text{m}^3 \text{mol}^{-1}$
$T_{\text{surf}}$	Surface temperature	573	K
$T_{\text{CMB}}$	CMB temperature	2467	K
$H$	Radiogenic heating rate	$4 \cdot 10^{-8}$	$\text{W m}^{-3}$
$B$	Buoyancy ratio	0.818	-

## 2. Methods

### 2.1. Governing Equations

We model the mantle as an anelastic, incompressible viscous shell without phase transitions. We also make the Boussinesq approximation, which simplifies the equations by assuming that variation in density enters into them only through the buoyancy term [e.g., *Christensen and Yuen, 1985; Roberts and Zhong, 2006*]. The mantle dynamics are thus governed by the following nondimensionalized equations for conservation of mass, momentum, and energy.

$$\nabla \cdot \vec{u} = 0 \quad (1)$$

$$-\nabla p + \nabla \cdot [\mu(\nabla \vec{u} + \nabla^T \vec{u})] + Ra(T - BC)\hat{r} = 0 \quad (2)$$

$$\frac{\partial T}{\partial t} + \vec{u} \cdot \nabla T = \nabla^2 T + H_{\text{int}} \quad (3)$$

where  $\vec{u}$  is the velocity,  $p$  is the pressure,  $\mu$  is the dynamic viscosity, and  $\hat{r}$  is the radial unit vector.  $T$  is temperature nondimensionalized to be zero at the top surface and one at the bottom surface. We define the thermal Rayleigh number  $Ra$  as

$$Ra = \frac{\rho_o g \alpha \Delta T R^3}{\kappa \mu_o} \quad (4)$$

where  $\rho_o$  is a reference density,  $g$  is gravitational acceleration, assumed here to be constant,  $\alpha$  is the thermal expansivity,  $\Delta T$  is the superadiabatic temperature difference across the entire model,  $R$  is the radius,  $\kappa$  is the thermal diffusivity, and  $\mu_o$  is the reference viscosity at the core-mantle boundary of the model. Note that our nondimensionalizations use  $R$  as the characteristic length scale rather than mantle thickness.

The buoyancy ratio  $B$  describes the relative size of density differences due to thermal expansion versus variation in chemical density,

$$B = \frac{\Delta\rho_{\text{ch}}}{\rho_o \alpha \Delta T}. \quad (5)$$

where  $\Delta\rho_{\text{ch}}$  is the density range due to composition alone.  $C$  is a nondimensional material property between 0 and 1, where  $C = 0$  denotes the least dense material and  $C = 1$  denotes the most dense material. The transport equation for the chemical composition field is described by

$$\frac{\partial C}{\partial t} + \vec{u} \cdot \nabla C = 0. \quad (6)$$

$H_{\text{int}}$  is the internal heating term, given by

$$H_{\text{int}} = \frac{QR^2}{c_p \Delta T \kappa}, \quad (7)$$

**Table 2.** Model Results: Morphology Calculations

Name	$Ra$	$E'$	Degree of Overturn
I8	$2.3 \cdot 10^8$	0	6
E2	$2.3 \cdot 10^8$	2	8
E3	$2.3 \cdot 10^8$	3	8
E4	$2.3 \cdot 10^8$	4	10
T8	$2.3 \cdot 10^8$	5	8

where  $Q$  is the volumetric heating rate. For simplicity, a constant internal heating is used. However, fractional crystallization would have concentrated radiogenic elements in the upper layer of the mantle, thereby reducing near-surface viscosity and facilitating the overturn process. We consider both

**Table 3.** Model Results: Timescale Calculations

Name	$Ra$	$E'$	Time at 80% Overturn Completion (Ma)	98% Completion (Ma)
I8	$2.3 \cdot 10^8$	0	5.38	22.2
I7.5	$2.3 \cdot 10^{7.5}$	0	16.5	61.5
I7	$2.3 \cdot 10^7$	0	51.9	159
I6.5	$2.3 \cdot 10^{6.5}$	0	156	369
I6	$2.3 \cdot 10^6$	0	443	733
T8	$2.3 \cdot 10^8$	5	960	1,820
T7.75	$2.3 \cdot 10^{7.75}$	5	2,440	4,160
T7.5	$2.3 \cdot 10^{7.5}$	5	4,520	9,450
T7	$2.3 \cdot 10^7$	5	22,400	42,700

the isoviscous case and a temperature- and pressure-dependent viscosity with an Arrhenius rheology, given by

$$\mu = \mu(T, z') = \mu_o \exp \left( \frac{E' + V'z'}{T + T_{off}} - \frac{E' + V'(1 - R'_{CMB})}{1 + T_{off}} \right) \quad (8)$$

where  $T_{off} = \frac{T_{surf}}{\Delta T}$ ,  $T_{surf}$  being surface temperature, and  $E'$ ,  $V'$ , and  $z'$  are nondimensionalized activation energy, activation volume, and depth, respectively [Roberts and Zhong, 2006].  $R'_{CMB}$  is the nondimensionalized radius of the core.  $\mu$  is capped at  $\mu = \mu_o \cdot 10^6$ . Tables 1–3 record the fixed and varied input parameters, respectively.

### 2.2. Model

The governing equations are solved with the finite element method using CitcomS, which performs these calculations in 3-D spherical geometry [Zhong et al., 2008]. The model, a spherical shell, is divided into 12 identically shaped caps. Each cap is divided into a  $48 \times 48 \times 48$  grid, at every node of which the equations are solved. For the Mars geometry assumed here, this results in a vertical resolution of about 40 km and a horizontal resolution of about 30 km at the CMB and 80 km at the surface. Calculations are distributed across 24 processors. Tracers, tracked particles spread throughout the model that are entrained in and move with the fluid flow, contain compositional density information used to calculate chemical buoyancy. Tracers also contain information on their initial position in the model, in order to differentiate between two materials with equal density but diverse mineralogy.

Both the bottom and the top boundaries of the shell are isothermal and free slip. These model boundaries correspond to the physical boundaries with atmosphere and liquid outer core, respectively, both of which are considered low-viscosity isothermal reservoirs over the timescales of interest. Thus, the model is cooled from above while being heated basally and internally. No crust is modeled.

### 2.3. Initial Conditions

Two sets of calculations are made. The first set models two-layer Rayleigh-Taylor overturn to test the results by Zhong and Zuber [2001] that predict an increased overturn wavelength with larger viscosity contrast and

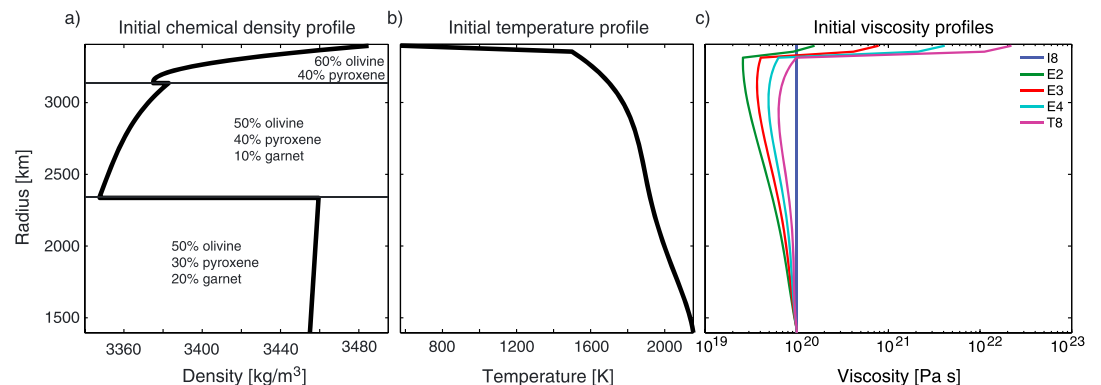


**Figure 1.** Initial conditions. (a) The thermal profile is the superadiabatic solidus temperature with a constant surface condition of 573 K. (b) The chemical density profile is the result of magma ocean solidification as calculated by Elkins-Tanton et al. [2005]. (c) Several viscosity rheologies were used to study the initial overturn. I8 (blue) and T8 (magenta), the isoviscous case and the case with the highest viscosity contrast, respectively, were continued and repeated with different Rayleigh numbers.

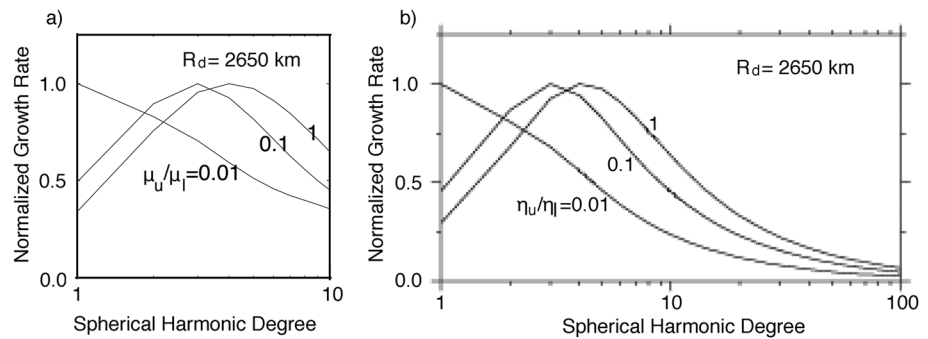


**Figure 2.** (a) The dependence of growth rate on degree of perturbation and viscosity contrast for an interface located at  $R = 2650$  km. (b) *Zhong and Zuber* [2001] results for comparison.

layer thickness. The second set models a more complex Rayleigh-Taylor instability scenario that could have arisen after the fractional solidification of a whole-mantle Martian magma ocean.

**2.3.1. Two-layer Rayleigh-Taylor Overturn**

In the two-layer calculations, an isoviscous high-density layer is initially underlain with an isoviscous low-density layer. All thermal aspects of the model are removed, such that all buoyancy is chemical. In this manner we can study the simple case of a two-layer Rayleigh-Taylor instability in three-dimensional spherical geometry. Two parameters that can affect wavelength of overturn are  $\mu_u/\mu_l$ , the ratio of viscosities of the top and bottom layers, and  $r_i$ , the radius of the interface between the layers.

First, calculations are run in which the interface is given an initial perturbation of varying degree  $l$  (order  $m = 0$ ). The fastest growing of these perturbations is the most unstable wavelength for the given viscosity and thickness parameters. Then, calculations are run which have no initial perturbation in the interface apart from small variations in density due to the randomized nature of tracer placement. These variations serve to initiate motion but do not appear to influence the resultant degree of overturn. The  $\mu_u/\mu_l$  and  $r_i$  are varied independently and the most unstable wavelength is recorded for each case.

**2.3.2. Overturn Model With Thermal and Chemical Profiles**

Next we use the full model which includes thermal buoyancy and a range of chemical densities. The initial chemical density is uniform laterally but varies continuously with depth. This initial density profile (Figure 1a) is the result of calculations of simple fractional crystallization reported in *Elkins-Tanton et al.* [2003] assuming that the entirety of the mantle was molten. The entire mantle is assumed to be at its solidus temperature after magma ocean solidification (Figure 1b). These two initial conditions can be made assuming the bulk of mantle ocean solidification occurs much quicker than convective and conductive timescales.

First we determine the harmonic degree of initial overturn that occurs provided five different viscosity profiles (Figure 1c) created by adjusting activation volume  $V'$  and activation energy  $E'$  in equation (8). The degree is calculated by making a spherical harmonic analysis of radial velocity at each depth and averaging their powers weighted by velocity magnitude.

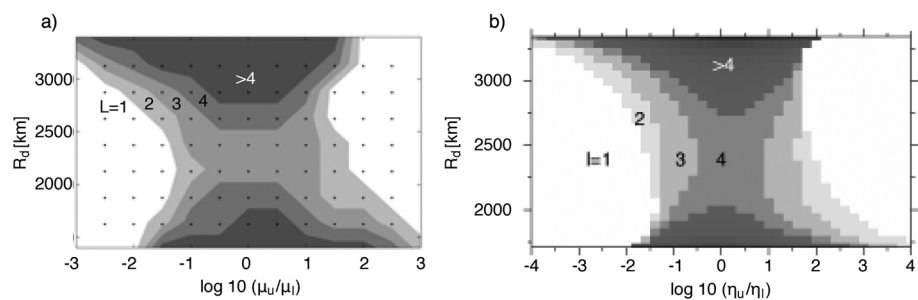


**Figure 3.** (a) The observed degree of overturn as a function of viscosity contrast and interface radius. At each black point, two calculations with randomized initial tracer location were made, and the average of their spherical harmonic decompositions were recorded. The contour lines are interpolated around those 77 points. (b) *Zhong and Zuber* [2001] results for comparison.

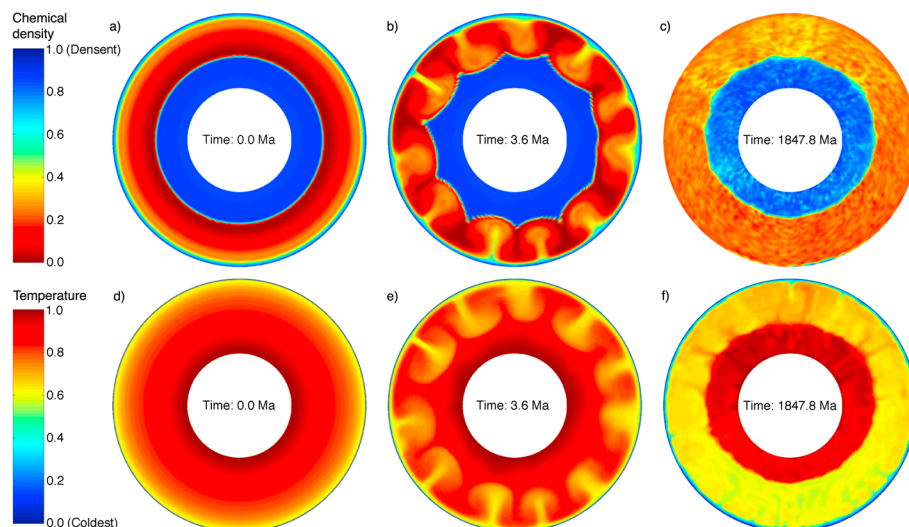


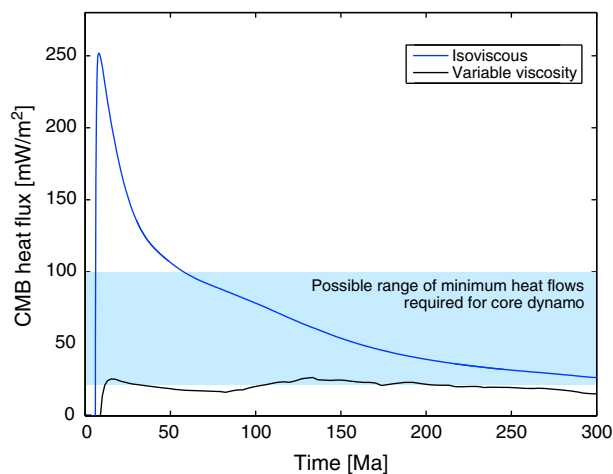
**Figure 4.** Overturn cross sections in (a–c) chemical density and (d–f) temperature for temperature- and pressure-dependent rheology case T8. The cross sections show the model at three times: initiation (Figures 4a and 4d), early overturn (Figures 4b and 4e), and completion of overturn (Figures 4c and 4f).

There are many possible metrics with which to measure the timescale of overturn. Here we choose to consider the density instability in the upper half of the mantle. We determine the time required for the density contrast across the unstable region to be reduced by 80%, and to be reduced by 98%. Thus, overturn is 80% complete when

$$d\rho_{ch} \leq 0.2\Delta\rho_{ch}, \tag{9}$$

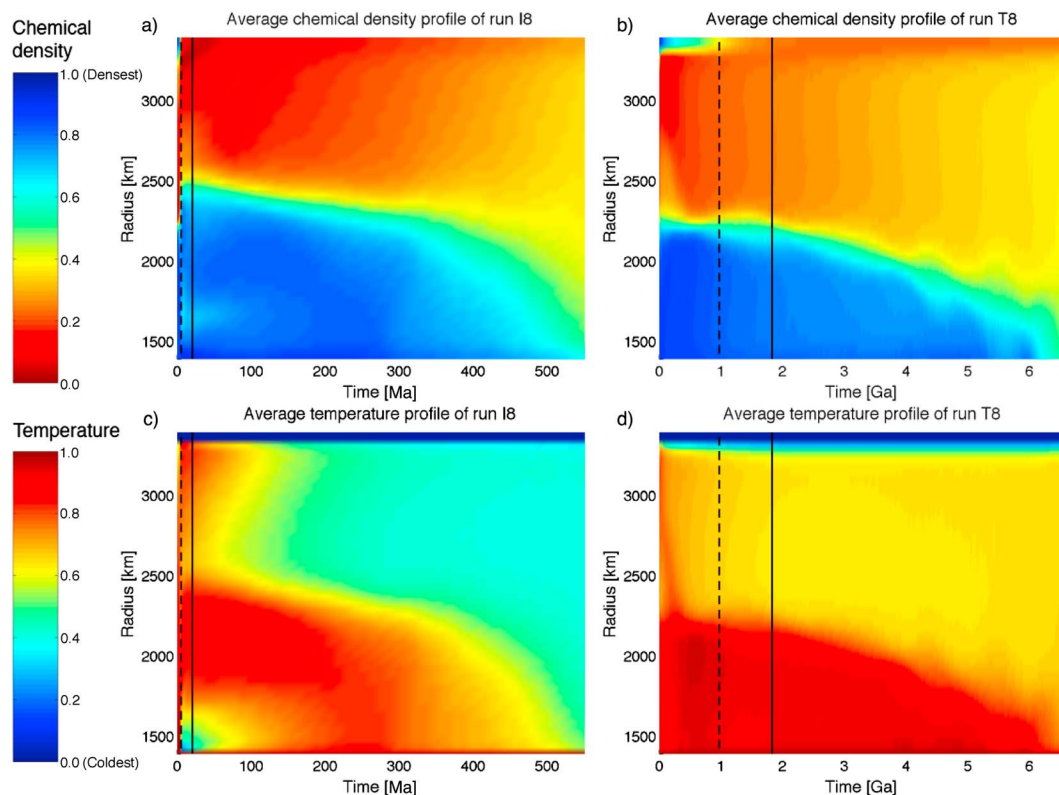
where  $d\rho_{ch}$ , the chemical density instability, decreases with time as overturn progresses.

The choice of rheology will fundamentally impact results. Experimentally determined mineral activation energies for diffusion creep range from 300 to 375 kJ/mol [Karato and Wu, 1993; Hirth and Kohlstedt, 2003]. However, Christensen [1984] showed that when assuming a Newtonian rheology, the effective activation energy should be lowered by multiplying a prefactor of 0.3–0.6 to approximate non-Newtonian effects. In the case of the early Martian mantle, several other factors could work to temporarily reduce viscosity in the upper mantle. First, since the material is at its solidus, some degree of partial melt could likely be present, reducing viscosity. Second, the presence of water can also lower viscosity by several orders of magnitude [e.g., Hirth and Kohlstedt, 1996]. Third, the gravitationally unstable upper layer would be enriched in radiogenic heat-producing elements. To demonstrate the effect of concentrated radiogenic heating, we construct a one-dimensional half-space diffusion model of the surface with concentrated radiogenic heating (Appendix A).



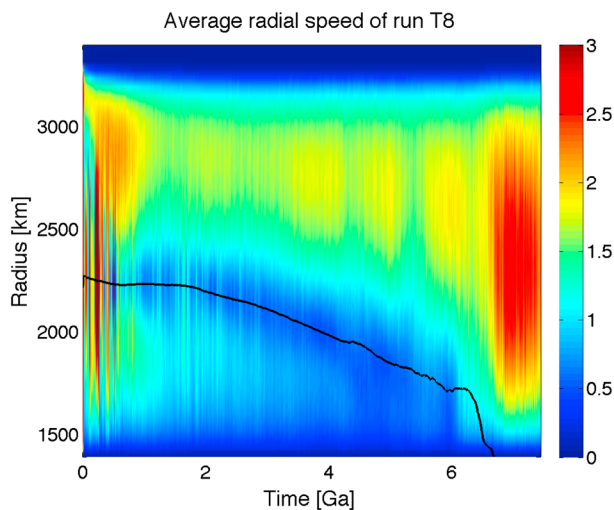
**Figure 5.** The initial impact on heat flux across the core-mantle boundary due to overturn for the temperature- and pressure-dependent rheology case T8 and the isoviscous case I8.

To demonstrate the effect of concentrated radiogenic heating, we construct a one-dimensional half-space diffusion model of the surface with concentrated radiogenic heating (Appendix A). As shown, cooling of the dense layers is significantly delayed. Combining these effects, a small viscosity contrast is plausible. We employ effective activation energies ranging from 0 kJ/mol (constant viscosity) to 78 kJ/mol



**Figure 6.** Horizontally averaged (a and b) chemical density and (c and d) temperature for two runs. The dashed vertical line marks the point at which the chemical density instability is 20% of its original size, while the solid line marks the point at which the instability is reduced to 2% its original size. The entrainment rate is poorly resolved in the numerical model and shown here for qualitative demonstration, although the timescale is fairly similar to that produced by scaling estimates.

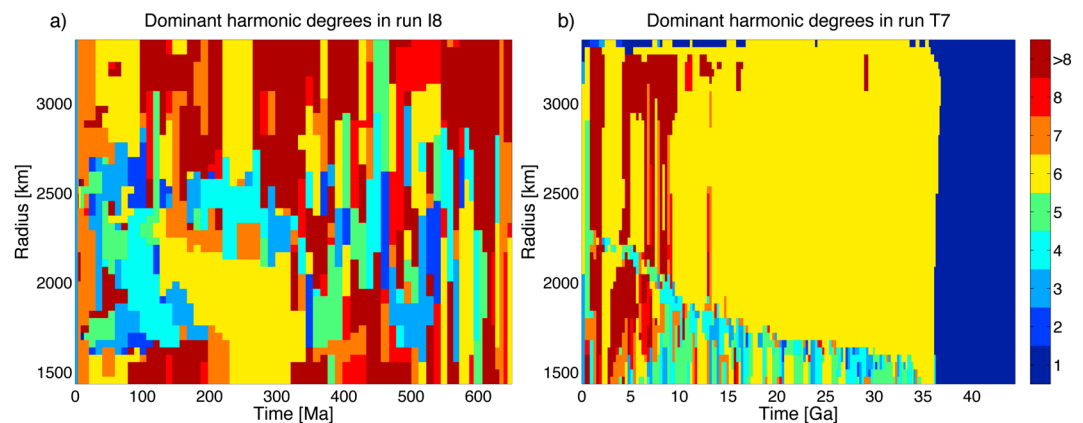
in order to study the results of the low viscosity contrasts shown in Figure 1c. A larger viscosity with a stagnant lid will effectively prevent the gravitationally unstable layer from overturning altogether.



**Figure 7.** Average radial speed. The black line shows the interface between the more chemically dense lower mantle material and the lighter upper mantle material. The low radial speeds along the interface indicate that two-layer convection occurs until the lower mantle material is entrained. The brief periods of high speed indicate that particularly strong advective activity is able to cross the otherwise conductive interface.

We choose a constant surface temperature of 300°C since the recently solidified magma ocean will be about 1200°C but will cool quickly. Surface temperature was varied and found to affect the overall dynamics minimally (Figure 12).

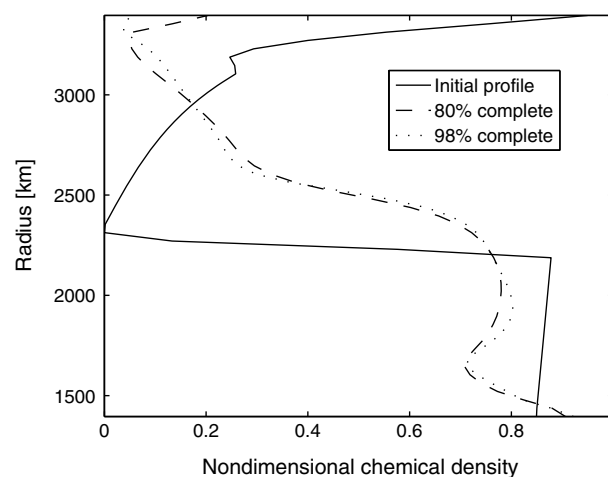
It is important to note that current models are unable to resolve systems with Rayleigh numbers corresponding to the viscosities possibly present in a recently solidified magma ocean. To address this issue, we use a scaling approach. We run models with several reference viscosities that produce manageable Rayleigh numbers ( $10^6$ – $10^8$ ) and extrapolate to lower viscosities. Thus, while the models use a large-dimensional timescale over which assumptions of constant boundary temperature and low-surface viscosity are not valid, the results can be scaled to apply to small timescales over which they are valid.



**Figure 8.** Most dominant harmonic degrees (in radial velocity) for (a) an isoviscous case (I8) and (b) a temperature- and pressure-dependent viscosity case (T7). Viscosity contrast resulted in degree-one convection but only after entrainment was complete.

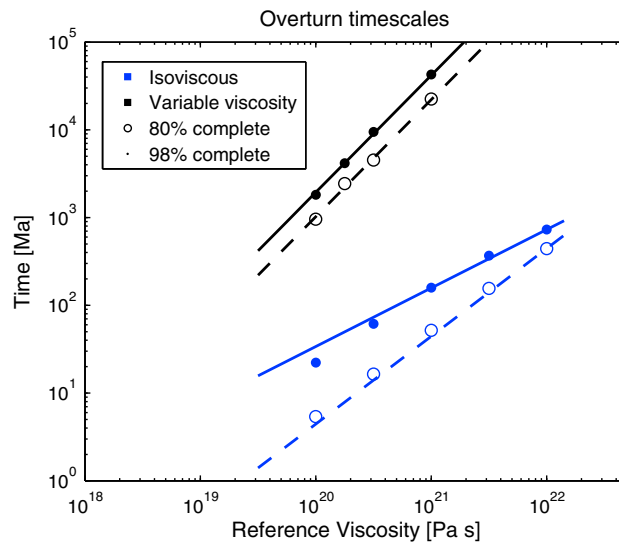
### 3. Results

Figure 2a shows example runs of the two-layer case in which a specific initial wavelength is introduced. These results are quantitatively and qualitatively consistent with the analytic solutions [Zhong and Zuber, 2001, Figure 2b]. Wavelengths were somewhat shorter than found by Ke and Solomatov [2006], who mapped characteristic wavelengths assuming a thin unstable layer near the core-mantle boundary (CMB). Figure 3a shows the dominant harmonic degree of overturn as a function of interface radius and viscosity ratio. Degree-one overturn occurs only when significant viscosity contrast exists between adjacent layers. The thinner a layer, the more contrast is necessary for degree-one. For the case of  $\mu_u/\mu_l = 1$ ,  $l = 3$  overturn is the lowest achievable degree of overturn, but only if the layers are sufficiently thick (Figure 3a). This is different from the analytical solution (Figure 3b), which predicts  $l = 4$  is the minimum achievable degree for those viscosity conditions; overall, however, our model matches the analytical solutions well qualitatively. Figure 3a was constructed from model calculations with a random initial perturbation, validating the assumption that the most unstable wavelength will generally come to dominate an overturn event.



**Figure 9.** Profiles of the horizontally averaged nondimensionalized chemical density from an isoviscous model (I8) initially and after the density instability in the upper layer of the mantle is reduced by 80% and 98%. The lower mantle develops a chemical density instability that is resolved slowly as cold but chemically light material that has fallen to the lower mantle warms conductively and rises back into the upper mantle. This late lower mantle process is not included in our assessment of overturn timescales.

For the predicted Martian thermal and chemical profiles, degree of overturn was more difficult to define than in the two-layer case, since there existed no well-defined interface on which to perform a spherical harmonic analysis, and since degree also tended to vary with time. However, degree-one overturn was not observed for any of the viscosity parameters used in Figure 1. Rather, as recorded in Tables 2 and 3, surface material arrived at the CMB in several cold, dense downwellings with a pattern of high degree ( $l = 5 - 9$ ). In all cases, a perturbation initiated at the depth at which the local ratio of buoyancy forces to viscous resisting was highest, then expanded to other depths. In the isoviscous case, overturn initiated at the surface. In the temperature- and pressure-dependent viscosity cases, it initiated where viscosity was lowest, at near 400 km depth (Figure 4b).



**Figure 10.** Timescales. Advection in early planetary history was likely too rapid to be resolved by present models. We can extrapolate to higher Rayleigh numbers (lower viscosity) using the trends determined from high-viscosity calculations. For example, assuming a realistic viscosity profile lies between isoviscous (*I*) and variable viscosity (*V*) as bounds and assuming a reference viscosity of  $10^{18}$  Pa s, overturn would have taken about 3–4 Ma.

ally mixing the entire mantle (Figure 6). During the entrainment period, convection occurs independently in the lower mantle as well, but the boundary between them is effectively conductive (Figure 7), i.e., layered convection [e.g., *Davaille, 1999*].

Short-wavelength convection patterns dominated during the entrainment phase in all models (Figure 8). In the isoviscous cases, small convection cells persist as the model continues into thermal convection. However, for the temperature- and pressure-dependent rheology, the transition to whole-mantle thermal convection was associated with the emergence of a degree-one convection pattern that persisted with stability as far as the model was run.

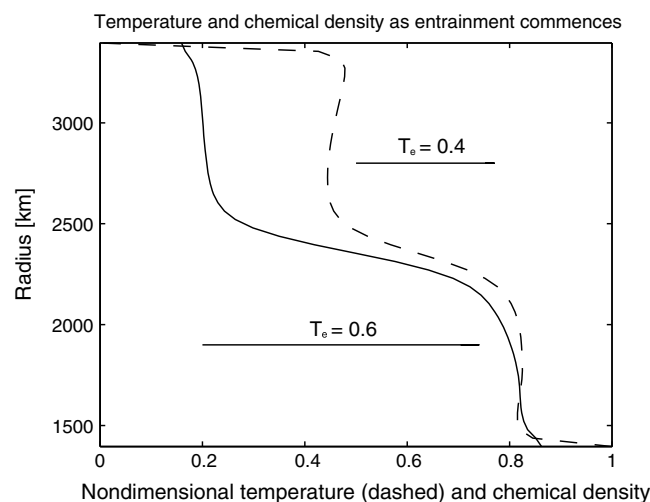


**Figure 11.** Horizontally averaged nondimensionalized chemical density and thermal profiles from an isoviscous model (I8) after overturn is complete and when thermal convection has homogenized the upper mantle enough to produce a well-defined two-layer system to which scaling arguments can be applied. The density and thermal contrasts in this figure are used to compute the buoyancy ratios used in our entrainment estimates.

Models using a higher activation energy (300 kJ/mol) resulted in a stagnant lid in the enriched upper 250 km that did not overturn. The upper mantle beneath the lid was able to invert and homogenize, but this inversion did not cause any notable effect on CMB heat flow.

In the isoviscous calculations, the dense surface material was able to descend directly to the CMB, causing a surge of heat flux from the core (Figure 5). For temperature-dependent rheologies, however, the high viscosity near the surface slowed the process. Material gradually seeped down, resulting in a smaller but more persistent overturn-induced heat flux. After initial overturn, the models stabilized into a dense lower mantle and a light upper mantle. Over time, convection in the upper region entrained dense material from underneath, eventu-

ally reaching the defined stages of completion in the isoviscous model. Because of its low temperature, some chemically light material was able to descend into the lower mantle despite having lower density. This effect created a small chemical density instability in the lower mantle, which reequilibrated gradually as the material was heated conductively to the temperature of its new surroundings. Figure 10 shows the timescales observed for overturn of the upper mantle. Three scalings were noted. First, 80% of overturn was complete in the isoviscous cases with timescale proportional to  $Ra^{-1}$ . Second, 98% was complete with timescale proportional to  $Ra^{-2/3}$ . Third, in the temperature- and pressure-dependent viscosity cases,

both overturn timescales scaled as  $Ra^{-4/3}$ . While the bulk of the high-density material descended quickly, the rate of this process slowed significantly as the density instability lessened.

### 3.1. Entrainment and Whole-Mantle Mixing

Although we show the entrainment process in Figure 6 for qualitative understanding, the actual entrainment rate is difficult to model with a global 3-D finite element framework since prohibitively high spatial resolution of upwellings is required for accurate results [van Keken *et al.*, 1997; Zhong and Hager, 2003]. Even using models with adaptive mesh refinement to several km grid resolution, it is difficult to resolve entrainment rate for temperature-dependent viscosity [Leng and Zhong, 2011]. Both laboratory and numerical experiments have been used to understand the mechanisms and timescale with which a convecting upper layer entrains underlying denser material [Davaille, 1999; Gonnermann *et al.*, 2002; Jellinek and Manga, 2002; Zhong and Hager, 2003]. Using the compositional and thermal profiles of our isoviscous model immediately after overturn, we use an experimentally derived scaling law to estimate the timescale over which the lower dense layer would survive.

Davaille [1999] experimentally derived a scaling theory for entrainment rate, further corroborated by later laboratory work [Gonnermann *et al.*, 2002], finding that

$$q = 0.2\kappa d^{-1} B_D^{-2} Ra_d^{1/3} \frac{1}{1 + \gamma B_D^{-1}}, \quad (10)$$

where  $q$  is entrainment flux per unit area and viscosity contrast  $\gamma$  is the viscosity ratio between the two layers. The buoyancy ratio defined by Davaille,  $B_D$ , includes the thermal buoyancy across the entire model, so equals  $B C_e$  (Figure 11).  $Ra_d$  is the Rayleigh number, with the subscript added to clarify that in this equation Rayleigh number is defined by mantle depth, not planetary radius. Applying this equation to our postoverturn profile, we estimate a lifetime of 500 Ma for an isoviscous ( $\gamma = 1$ ) scenario, and 3.8 Ga for  $\gamma = 10$ . The entrainment timescales of our numerical models, albeit insufficiently resolved, were a similar magnitude.

## 4. Discussion

The absence of degree-one overturn pattern suggests that cumulate overturn may not play the hypothesized role of initiating a hemispherical core dynamo or contributing to the crustal dichotomy. We can understand the difficulty in creating a degree-one pattern by closer consideration of the two-layer case. Long-wavelength instabilities occur more easily when viscosity contrast is high and when both layers are of a substantial thickness compared with total model thickness. Although these conditions can be easily reached in a two-layer system, any scenario in which viscosity and chemical density vary continuously and gradually with depth will not satisfy those requirements. Parmentier *et al.* [2002] found that for the Moon, degree-one overturn is possible when a large viscosity contrast occurs over a small depth range when a high-density layer is placed on a uniform density mantle. In our scenario however, the density instability was gradual across a large range. Because overturn initiates wherever buoyancy forces face the least resistance from viscosity, any large contrast in viscosity between two layers will, rather than increasing wavelength, force the overturn to occur at some other depth at which both the upper and lower layers are of relatively low viscosity. Additionally, the initially overturning layers will tend to be thin, since material surrounding the minimum in viscosity is by definition of higher viscosity, and therefore slower to join in the overturn. Thus, the initial overturn will always occur in a thin layer of a region with low viscosity contrast, and will always invert in a short-wavelength pattern.

Although degree-one overturn may be unlikely, previous work [Zhong and Zuber, 2001; Roberts and Zhong, 2006] has demonstrated the tendency toward degree-one convection when a more realistic asthenosphere and lithosphere rheology is included. In this study, we found that subsequent single-cell convection was a consistent result after complete entrainment of the dense lower layer when viscosity varied with temperature, but the hemispherical dichotomy on Mars would have predated the completion of entrainment even using our shortest estimates of entrainment timescale. Ke and Solomatov [2009] suggest an independent mechanism for degree-one convection, a superplume originating from a thermal Rayleigh-Taylor instability at the core-mantle boundary, which could also potentially induce and sustain degree-one convection.

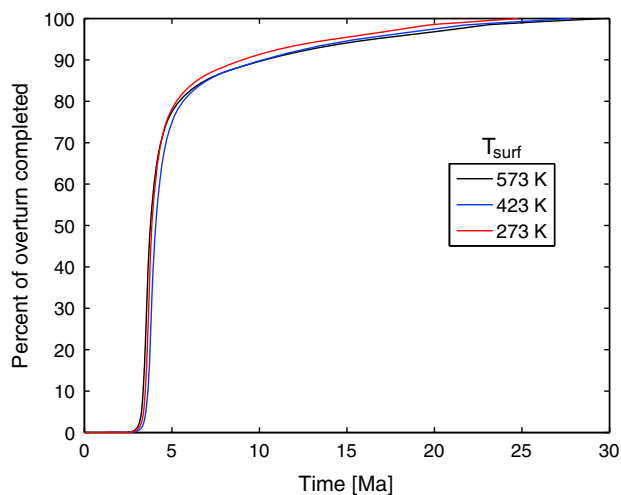


**Figure 12.** Normalized size of density instability as a function of time for the isoviscous case I8 for varied surface temperature. Changes in the surface boundary condition do not significantly alter the resultant timescales and scaling properties.

Rheological assumptions play a large role in determining the rate of overturn. While our temperature-dependent model had a viscosity contrast of around 1000:1, a higher contrast would extend the lifetime of a gravitationally unstable lithosphere, delaying mixing and permitting a relatively isolated chemical reservoir enriched in incompatible elements by fractional crystallization.

There are three end-member scenarios for the fate of the heavy-element-enriched layer resulting from late-stage fractional crystallization: that it was not able to overturn at all; that overturn occurred and the stable density stratification was not overcome by convection; or that the whole mantle became well mixed. However, gravity and moment of inertia observations do not support the

possibility of an extant high-density stagnant lid [Pauer and Breuer, 2008; Sohl and Spohn, 1997].

Assuming overturn did occur, the lower layer could have been entrained significantly, creating isotopic heterogeneities throughout the mantle. Later melting events responsible for crustal formation would therefore have access to the full range of isotopic signatures formed during fractional solidification, accounting for the differences in isotopic signatures found between SNC meteorites. Mixing would bring small-scale reservoirs near the surface where that would be more readily possible.

The extent to which mixing has occurred is poorly constrained. Employing empirically derived scaling laws, we calculated the lifetime of a dense lower layer after overturn in an isoviscous mantle to be 500 Ma and 3.8 Ga if the upper mantle were ten times more viscous than the lower mantle. Since these results do not scale strongly with Rayleigh number, uncertainty in  $Ra$  should not affect them significantly. However, a stagnant lid and secular cooling across long timescales will slow later entrainment and extend the lifetime of the

dense lower layer significantly. Tosi *et al.* [2013] showed that for a Mars overturn scenario with an inverted linear density gradient, complete mixing by present day is unlikely.

The scaling properties evident in Figure 10 are of particular interest. In a Rayleigh-Taylor overturn process with no thermal processes, timescale is proportional to mantle viscosity, or  $Ra^{-1}$ . The  $Ra^{-2/3}$  and  $Ra^{-4/3}$  time scalings observed in isoviscous and temperature-dependent models, respectively, suggests that thermal mechanisms play a large role in opposing or reinforcing the gravitational instability.

Our results suggest in an isoviscous mantle, the bulk of overturn occurs quickly enough that thermal diffusion is not an important process for it, resulting in a  $Ra^{-1}$  time scaling, while the remaining

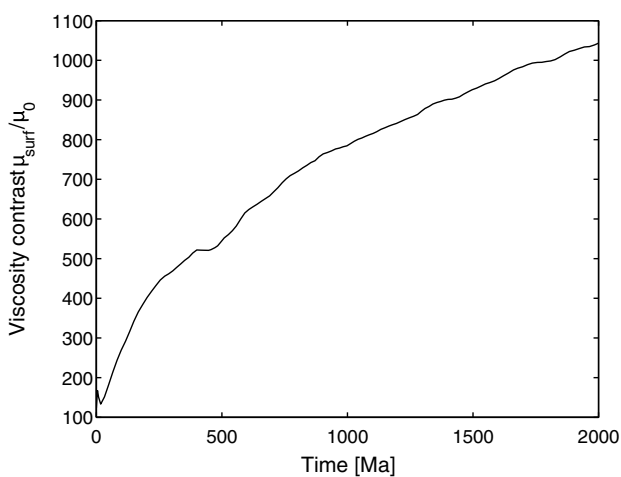


**Figure 13.** The ratio of viscosity in the uppermost element of the model to reference viscosity for the temperature-dependent viscosity model T8 with reference viscosity  $\mu_0 = 10^{20}$  Pa s. As the lithosphere cools conductively, viscosity in the surface elements increases. The smaller the Rayleigh number, the more pronounced the effect of this viscosity increase on overturn timescales, producing timescales proportional to  $Ra^{-4/3}$ .

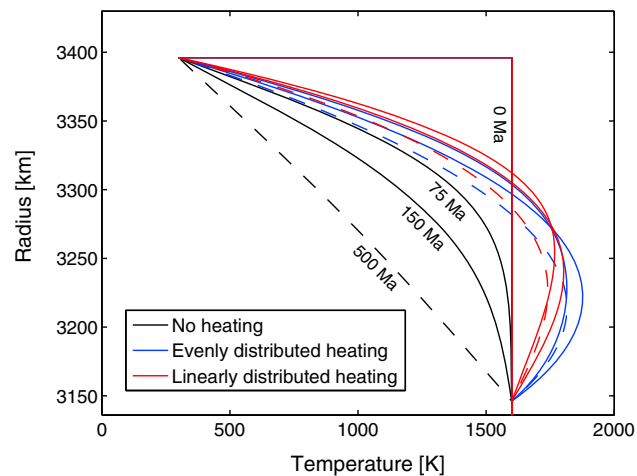


**Figure A1.** Temperature profiles for a 1-D finite difference model of the upper 250 km of the mantle. In the absence of concentrated radiogenic heating, conductive cooling quickly creates a stagnant lid. With radiogenic heating accounted for, high temperatures are prolonged enough that the high-density surface material will likely sink.

A theoretical derivation of this  $Ra^{-4/3}$  scaling is needed but beyond the scope of this study. We expect that for high Rayleigh numbers, diffusion will again no longer play a significant role, resulting in a  $Ra^{-1}$  timescale. However, for Rayleigh numbers that we were able to resolve, we did not reach this regime.

Surface temperature and core temperature were constant in our model. In reality, both these variables decrease with time, so that this assumption, although valid for timescales on the order of 100 Ma, may be less valid with larger timescales. Cooling will increase viscosity with time, while a decrease in the temperature contrast across the mantle will reduce thermal buoyancy. Thus, if thermal convection is unable to overcome a chemical density profile early on, complete entrainment might not be possible.

## 5. Conclusion

We present four broad conclusions:

1. The harmonic degree of overturn varies between 6 and 10 for the cases examined here that assume a sluggish rather than stagnant lid. We therefore conclude that degree-one overturn is unlikely to have resulted from magma ocean fractional crystallization in Mars or other planets with the characteristics explored here.
2. An initial overturn event could create an added core heat flux in excess of tens of mW during the period of stability prior to the onset of thermal convection.
3. For an isoviscous mantle with  $\mu_o = 10^{20}$  Pa s, a dense lower layer produced by fractional crystallization and subsequent overturn would persist on the order of 500 Ma. A viscosity contrast of 10 between the lower and upper mantle would increase this lifetime to 3.8 Ga. Secular cooling and a stagnant lid will extend timescales further. Complete mixing of chemically homogenous has therefore likely not occurred, but there would have been sufficient entrainment to permit smaller-scale domains of isotopically distinct material to participate in melting and crustal formation.
4. Thermal processes strongly impact the Rayleigh-Taylor problem in most scenarios. Overturn timescales in models assuming constant viscosity scale as  $Ra^{-1}$  for the bulk of overturn but  $Ra^{-2/3}$  for the remainder. Overturn times scale as  $Ra^{-4/3}$  when using a temperature- and pressure-dependent rheology. Provided the range of rheologies examined here and given  $\mu_o = 10^{19}$  Pa s, 98% of overturn would have taken 7–90 Ma. For  $\mu_o = 10^{18}$  Pa s, the process would have required about 2–4 Ma.

20% takes several times longer (Figure 12). However, the descent of the final 20% of the chemically dense upper layer will scale with  $Ra^{-2/3}$  since the surface material has time to become more negatively buoyant through conductive cooling. For high Rayleigh numbers, thermal diffusion should become less relevant, and the final 20% of overturn should occur with the same Rayleigh number dependence as the initial 80%.

In contrast, when viscosity is temperature dependent, thermal diffusion slows down the overturn process rather than accelerating it. If the Rayleigh number is lowered, the upper layer has more time to cool conductively before advection of the unstable material occurs. This increased cooling raises the local viscosity (Figure 13), slowing advection further.

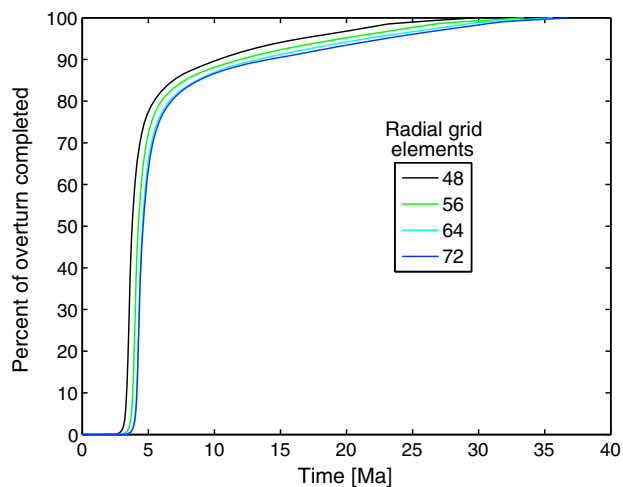


**Figure B1.** Normalized size of density instability as a function of time for the isoviscous case I8. Increasing resolution of each of the twelve-model caps from a  $48 \times 48 \times 48$  grid to a  $72 \times 72 \times 72$  grid alters results slightly, but the change is convergent. While resolution may cause the prefactor to differ, the observed scalings are robust.

distributed evenly into the upper 250 km of Mars, they would be about 4.9 times chondritic abundance. We consider an even distribution and a distribution increasing monotonically with radius.

The results are shown in Figure A1. Without internal heating, the solution is an error function. If concentrated radiogenic heating is present, high temperatures, and thus low viscosities, will persist for hundreds of Ma.

## Appendix B: Resolution

Figure B1 demonstrates the dependence of overturn time on resolution. Timescales differed slightly between high-resolution and low-resolution results. While resolution may cause the prefactor to differ, the observed scalings are robust.

## References

- Andrews-Hanna, J. C., M. T. Zuber, and W. B. Banerdt (2008), The Borealis basin and the origin of the Martian crustal dichotomy, *Nature*, *453*, 1212–1215.
- Borg, L. E., L. E. Nyquist, L. A. Taylor, H. Wiesmann, and C.-Y. Shih (1997), Constraints on Martian differentiation processes from Rb-Sr and Sm-Nd isotopic analyses of the basaltic shergottite QUE 94201, *Geochim. Cosmochim. Acta*, *61*, 4915–4931.
- Christensen, U. R. (1984), Convection with pressure- and temperature-dependent non-Newtonian rheology, *Geophys. J. R. Astron. Soc.*, *77*, 343–384.
- Christensen, U. R., and D. A. Yuen (1985), Layered convection induced by phase transitions, *J. Geophys. Res.*, *90*, 291–300.
- Davaille, A. (1999), Simultaneous generation of hotspots and superswells by convection in a heterogeneous planetary mantle, *Nature*, *402*, 756–760.
- Debaille, V., Q. Z. Yin, A. D. Brandon, and B. Jacobsen (2008), Martian mantle mineralogy investigated by the  $^{176}\text{Lu}$ - $^{176}\text{Hf}$  and  $^{147}\text{Sm}$ - $^{143}\text{Nd}$  systematics of shergottites, *Earth Planet. Sci. Lett.*, *269*, 186–199.
- Elkins-Tanton, L. T. (2008), Linked magma ocean solidification and atmospheric growth for Earth and Mars, *Earth Planet. Sci. Lett.*, *271*, 181–191.
- Elkins-Tanton, L. T., E. M. Parmentier, and P. C. Hess (2003), Magma ocean fractional crystallization and cumulate overturn in terrestrial planets: Implications for Mars, *Meteorol. Planet. Sci.*, *38*, 1753–1771.
- Elkins-Tanton, L. T., S. E. Zaranek, E. M. Parmentier, and P. C. Hess (2005), Early magnetic field and magmatic activity on Mars from magma ocean cumulate overturn, *Earth Planet. Sci. Lett.*, *236*, 1–12.
- Gonnermann, H. M., M. Manga, and A. M. Jellinek (2002), Dynamics and longevity of an initially stratified mantle, *Geophys. Res. Lett.*, *29* (10), 1399, doi:10.1029/2002GL014851.
- Hirth, G., and D. L. Kohlstedt (1996), Water in the oceanic upper mantle: Implications for rheology, melt extraction and the evolution of the lithosphere, *Earth Planet. Sci. Lett.*, *144*, 93–108.
- Hirth, G., and D. L. Kohlstedt (2003), Rheology of the upper mantle and the mantle wedge: A view from the experimentalists. Inside the subduction factory, *Geophys. Monogr.*, *138*, 83–105.
- Jellinek, A. M., and M. Manga (2002), The influence of a chemical boundary layer on the fixity, spacing and lifetime of mantle plumes, *Nature*, *41*, 760–763.
- Jones, J. H. (1986), A discussion of isotopic systematics and mineral zoning in the shergottites: Evidence for a 180 Myr igneous crystallization age, *Geochim. et Cosmochim. Acta*, *50*, 969–977.

## Appendix A: One-Dimensional Thermal Code

To demonstrate how radiogenic heating can maintain a high temperature in a lid produced by magma ocean solidification, we construct a 1-D conductive finite difference model of the upper 250 km of Mars governed by

$$\frac{\partial T}{\partial t} = \nabla^2 T + H_{\text{int}}. \quad (\text{A1})$$

The surface temperature is fixed at 300 K. The initial temperature everywhere else is 1600 K, and the base of the model at 250 km is fixed at this value. We assume initial chondritic values of radiogenic elements K, Th, and U, which become concentrated into the residual melt as fractional crystallization proceeds. If dis-

## Acknowledgments

This research is supported by an NSF Astronomy CAREER award. We thank Brad Hager and Marc Parmentier for useful discussion.

- Karato, S.-I., and P. Wu (1993), Rheology of the upper mantle: A synthesis, *Science*, *260*, 771–778.
- Ke, Y., and V. S. Solomatov (2006), Early transient super plumes and the origin of the Martian crustal dichotomy, *J. Geophys. Res.*, *111*, E10001, doi:10.1029/2005JE002631.
- Ke, Y., and V. S. Solomatov (2009), Coupled core-mantle thermal evolution of early Mars, *J. Geophys. Res.*, *114*, E07004, doi:10.1029/2008JE003291.
- Leng, W., and S. Zhong (2011), Implementation and application of adaptive mesh refinement for thermochemical mantle convection studies, *Geochem. Geophys. Geosyst.*, *12*, Q04006, doi:10.1029/2010GC003425.
- Marsh, B. D. (1995), Solidification fronts and magmatic evolution, *Mineral. Mag.*, *60*, 5–40.
- Martin, D., and R. Nokes (1989), A fluid-dynamic study of crystal settling in convecting magmas, *J. Petrol.*, *30*, 1471–1500.
- Parmentier, E. M., S. Zhong, and M. T. Zuber (2002), Gravitational differentiation due to initial chemical stratification: Origin of lunar asymmetry by the creep of dense KREEP, *Earth Planet. Sci. Lett.*, *201*, 473–480.
- Pauer, M., and D. Breuer (2008), Constraints on the maximum crustal density from gravity topography modeling: Applications to the southern highlands of Mars, *Earth Planet. Sci. Lett.*, *276*, 253–261.
- Righter, K., R. J. Hergiv, and D. A. Kring (1998), Accretion and core formation on Mars: Molybdenum contents of melt inclusion glasses in three SNC meteorites, *Geochim. et Cosmochim. Acta*, *62*, 2167–2177.
- Roberts, J. H., and S. Zhong (2006), Degree-1 convection in the Martian mantle and the origin of the hemispheric dichotomy, *J. Geophys. Res.*, *111*, E06013, doi:10.1029/2005JE002668.
- Sohl, F., and T. Spohn (1997), The interior structure of Mars: Implications from SNC meteorites, *J. Geophys. Res.*, *102*(E1), 1613–1635.
- Solomatov, V. S. (2000), Fluid dynamics of a terrestrial magma ocean, in *Origin of the Earth and Moon*, edited by R. M. Canup and K. Righter, pp. 323–338, Univ. of Ariz. Press, Tucson.
- Solomon, S. (1979), Formation, history, and energetics of cores in the terrestrial planets, *Phys. Earth Planet. Inter.*, *19*, 168–182.
- Stanley, S., L. T. Elkins-Tanton, M. T. Zuber, and E. M. Parmentier (2008), Mars paleomagnetic field as the result of a single-hemisphere dynamo, *Science*, *321*, 1822–1825.
- Tonks, W. B., and H. J. Melosh (1993), Magma ocean formation due to giant impacts, *J. Geophys. Res.*, *98*, 5319–5333, doi:10.1029/92JE02726.
- Tosi, N., A.-C. Plesa, and D. Breuer (2013), Overturn and evolution of a crystallized magma ocean: A numerical parameter study for Mars, *J. Geophys. Res. Planets*, *118*, 1512–1528, doi:10.1002/jgre.20109.
- Treiman, A. H., J. D. Gleason, and D. D. Bogard (2000), The SNC meteorites are from Mars, *Planet. Space Sci.*, *48*, 1213–1230.
- van Keken, P. E., S. D. King, H. Schmeling, U. R. Christensen, D. Neumeisters, and M.-P. Doin (1997), A comparison of methods for the modeling of thermochemical convection, *J. Geophys. Res.*, *102*, 22477–22496.
- Wetherill, G. W. (1990), Formation of the Earth, *Ann. Rev. Earth Planet. Sci.*, *18*, 205–256.
- Wetherill, G. W., and S. Inaba (2000), Planetary accumulation with a continuous supply of planetesimals, *Space Sci. Rev.*, *92*, 311–320.
- Zaraneck, S., and E. M. Parmentier (2004), Convective cooling of an initially stably stratified fluid with temperature dependent viscosity, *J. Geophys. Res.*, *109*, B03409, doi:10.1029/2003JB002462.
- Zhong, S., and M. T. Zuber (2001), Degree-1 convection mantle convection and the crustal dichotomy on Mars, *Earth Planet. Sci. Lett.*, *189*, 75–84.
- Zhong, S., and B. H. Hager (2003), Entrainment of a dense layer by thermal plumes, *Geophys. J. Int.*, *154*, 666–676.
- Zhong, S., A. K. McNamara, E. Tan, L. Moresi, and M. Gurnis (2008), A benchmark study on mantle convection in a 3-D spherical shell using CitcomS, *Geochem. Geophys. Geosyst.*, *9*, Q10017, doi:10.1029/2008GC002048.
- Zuber, M. (2001), The crust and mantle of Mars, *Nature*, *412*, 220–226.